Communications on Applied Nonlinear Analysis
ISSN: 1074-133X
Vol 32 No. 2 (2025)

Darcy-Forchheimer Flow of Casson Nanofluids Towards a Spinning Disk with Non-Uniform Heat Source

Chepiala Pushpalata[1], M. Monica[2], K. Satyanarayana[3], Ch. Kishore Kumar[4], B. Shankar[5], Mattipelli Ramachandru[6*]

[1]Department of Mathematics, TSWRDCW, Siddipet, Telangana, India-502103, ch.pushpalatha14@yahoo.com

[2]Department of Mathematics, TSWRDCW, Vikarabad, Telangana, India-501504, monica.medikare@gmail.com

[3]Department of Mathematics, UCS, Osmania University, Telangana, India-500007, satyamaths123@gmail.com

[4]Department of Mathematics, Nizam College (A), Hyderabad, Telangana, India-500001, kishoresai09@gmail.com

[5]Department of Mathematics, CVR College, Hyderabad, Telangana, India-501510, bandarishanker@yahoo.co.in

[6*]Department of Humanities &science, UCET, Mahatma Gandhi University, Telangana, India-508254, ramanmaths7@gmail.com

[*]Corresponding Author: Email: ramanmaths7@gmail.com

Article History:

Received: *28-07-2024*

Revised: *08-09-2024*

Accepted: *17-09-2024*

Abstract:
This study investigates the Darcy-Forchheimer flow of a Casson nanofluid over a spinning disk, incorporating the effects of a non-uniform heat source. Such flows are significant in various industrial and engineering applications, including cooling systems, lubrication technologies, and chemical processing involving complex fluids. The governing boundary layer equations, initially in partial differential form, were transformed into a set of ordinary differential equations (ODEs) using similarity transformations. These ODEs were then solved numerically using the bvp4c MATLAB solver. The influence of various physical parameters on the velocity, temperature, and concentration profiles was thoroughly analyzed and visualized through graphs. Additionally, the Nusselt and Sherwood numbers were computed and presented in tabular form to quantify heat and mass transfer rates.

Keywords: Darcy Forchhiemer, Casson fluid, nanoparticles, spinning disk, non-uniform Heat source.

1. Introduction

Non-Newtonian fluids have special flow characteristics that make them useful in many industrial applications, such as coating sheets, polymers, and optical fibers. Additionally, because of their capacity to withstand flow under stress, these fluids are essential to brake and damper systems. A particular kind of non-Newtonian fluid called Casson fluid has drawn a lot of interest recently because of its unique behavior, which makes it useful in situations where elastic and viscous qualities are equally relevant. Copley [1] and Blair [2] illustrated the fundamental shear characteristics of blood in arteries by employing the Casson fluid model. This fluid model stated to fit rheological data. According to the study of Nadeem et al. [3] and Kandasamy and Pai [4] Casson fluid exhibits the yield stress. The analytical study of the non-co-axial effects of transportation of mass subjected to first-order chemical reaction was examined by Jabbar et al. [5] Recently the numerical simulation of non-coaxial rotation of a Casson fluid towards a circular disc was examined by Alqarni et al. [6].

The study of the flow over rotating disk involves numerous industrial applications like Turbine disks, rotary type machine systems and application of rotating disk boundary-layer flow finds direct use in Chemical Vapour Deposition (CVD) reactors. The immense applications of this area attract many researchers. Von Karman [7] was the first one to give a prominent result on boundary layer flow over a rotating disk. He gave a differential equation model for the flow problem by using the appropriate integral procedure. Inspired by his study, Cochran [8] has found a series solutions for the same problem. Later, Benton [9] has improved Cochran's problem by considering the time-dependent case. Freidoonimehra et al. [10] discussed the behavior of MHD flow over a porous rotating disk using a semi-numerical/analytical method called HAM. Whereas a numerical solution for the Buongiorno model for the flow over a rotating disk along with velocity, thermal, and solutal slips was found by Mustafa [11]. Shehzad et al. [12] numerically explored the flow of a rotating disk in both upward and downward motion. Recently, the irreversibility analysis of flow of a hybrid nanofluid through a rotating disk by considering thermal radiation and magnetic field was done by Kumar & Mondal [13]. Different from the regular, Ali et al. [14] studied the unsteady hydro magnetic flow towards an inclined rotating disc by using the neural network approach.

At high velocities, fluid flow through porous medium becomes nonlinear, a phenomenon known as the Forchheimer effect. It incorporates inertial effects and goes beyond Darcy's law. By predicting fluid flow in densely packed, low-porosity reservoirs, it aids in oil recovery and maximises extraction. It helps to improve the quality of the final product in ceramic processing by helping to understand flow resistance in complicated, low-porosity materials. In non-Newtonian situations, when normal flow models are inadequate, it is useful overall. It occurs when there is a tightly packed medium with a lower porosity. A study conducted by Shenoy [15] examined the mixed, natural, and forced convection phenomena that can occur in non-isothermal structures. They were immersed in a type of porous medium that was saturated with a power-law fluid. Later, the two-dimensional Darcy-Forchheimer flow of Maxwell fluid towards a convectively heated sheet was studied by Sadiq & Hayat [16]. A study conducted by Vishnu Ganesh et al. [17] analyzed the effects of ohmic dissipations, second-order slip, and viscosity on the hydro magnetic nanofluid's flow in a porous medium. They found that the flow was directed toward a shrinking or stretching surface. Sadiq et al. [18] performed a similar study by using the Darcy-Forchheimer model on a convectively heated sheet. In a study by Khan et al. [19], they determined the optimal flow rate for the Carreau-Yasuda fluid on a flat surface with first-order velocity slip and Darcy-Forchheimer flow. A study conducted by Rasool et al. [20] revealed the influence of copper and alumina on the flow behavior of an electromechanical nanofluid made up of motor oil through a porous media known as Darcy-Forchheimer.

After the thorough examination, practically the high porosity was involved in the case of non-Newtonian fluids, which are hard to find out, and therefore, the Brinkman effects are not important while dealing with non-Newtonian fluids. Hence, in the present study we have considered the Darcy-Forchheimer model for the Casson fluid over a rotating disk to get better results.

2. Mathematical Formulation

Consider a 3D steady magnetohydrodynamic (MHD) Fluid dynamics is involved in the study of the motion of Casson Nanofluid, which is a semiconducting suspension of metallic particles at the Nano

scale. Particular issues pertaining to the slip dynamics have been identified. The angular velocity Ω and constants of the disk determine its rotation at z = 0. The electric field's influence can also be observed due to the Hall current.

Rheological of casson fluid is as follows Nayak et al., [21] and Waqas et al. [22].

$$\tau_{ij} = \begin{cases} 2\left(\mu B + \frac{P_y}{\sqrt{2\pi}}\right) e_{ij} \; ; \pi > \pi_c \\ 2\left(\mu B + \frac{P_y}{\sqrt{2\pi_c}}\right) e_{ij}; \; \pi < \pi_c \end{cases} \tag{1}$$

Here e_{ij} denotes the rate component of $(i,j)^{th}$, π denotes the product component of the deformation rate itself, π_c is based upon non- Newtonian relation, P_y denotes fluid yield- stress and μBdenotes non-Newtonian relation fluid plastic dynamic-Viscosity. If $\pi < \pi_c$ expression (1) can be modified into $\tau_{ij} = \mu B(\left(1 + \frac{1}{\gamma}\right) 2e_{ij}$. The upper half of plate is filed with nano fluid. The surface temperature T_w is higher than the ambient fluid temperature T_∞. The volumetric concentration C_w for ambient fluid isC_∞ .The radiation is also embedded in the energy equation profile in the existence of Thermophoretic and Brownian diffusion effects. Boundary conditions were considered. The heat flow activation energy from C-C in a porous material was also studied.

The governing equations are Waqas et al. [22] and Lv et al. [23]

$$\frac{\partial u}{\partial r} + \frac{u}{r} + \frac{\partial w}{\partial z} = 0 \tag{2}$$

$$\rho_f \left(u\frac{\partial u}{\partial r} - \frac{v^2}{r} + w\frac{\partial u}{\partial z}\right) = -\frac{\partial P}{\partial r} + \mu_f \left(1 + \frac{1}{\beta}\right)\left(\frac{\partial^2 u}{\partial r^2} + \frac{1}{r}\frac{\partial u}{\partial r} - \frac{u}{r^2} + \frac{\partial^2 u}{\partial z^2}\right) - \sigma_f B_0^2 u - \frac{\nu}{k^*}u - F_r u^2 \tag{3}$$

$$\rho_f \left(u\frac{\partial v}{\partial r} + \frac{uv}{r} + w\frac{\partial v}{\partial z}\right) = \mu_f \left(1 + \frac{1}{\beta}\right)\left(\frac{\partial^2 v}{\partial r^2} + \frac{1}{r}\frac{\partial v}{\partial r} - \frac{\nu}{r^2} + \frac{\partial^2 v}{\partial z^2}\right) - \sigma_f B_0^2 v - \frac{\nu}{k^*}v - F_r v^2 \tag{4}$$

$$\rho_f \left(u\frac{\partial w}{\partial r} + w\frac{\partial w}{\partial z}\right) = -\frac{\partial P}{\partial z} + \mu_f \left(1 + \frac{1}{\beta}\right)\left(\frac{\partial^2 w}{\partial r^2} + \frac{1}{r}\frac{\partial w}{\partial r} + \frac{\partial^2 w}{\partial z^2}\right) \sigma_f B_0^2 w - \frac{\nu}{k^*}w - F_r w^2 \tag{5}$$

$$u\frac{\partial T}{\partial r} + w\frac{\partial T}{\partial z} = \alpha_m \left(\frac{\partial^2 T}{\partial r^2} + \frac{\partial^2 T}{\partial z^2} + \frac{1}{r}\frac{\partial T}{\partial r}\right) + \frac{(\rho c)_p}{(\rho c)_f}\left\{D_B\left(\frac{\partial T}{\partial r}\frac{\partial C}{\partial r} + \frac{\partial T}{\partial z}\frac{\partial C}{\partial z}\right) + \frac{D_T}{T_\infty}\left(\left(\frac{\partial T}{\partial r}\right)^2 + \left(\frac{\partial T}{\partial z}\right)^2\right)\right\} -$$
$$\lambda_2 \left(u^2\frac{\partial^2 T}{\partial r^2} + w^2\frac{\partial^2 T}{\partial z^2} + 2uw\frac{\partial^2 T}{\partial r \partial z} + \left(u\frac{\partial u}{\partial r} + w\frac{\partial u}{\partial z}\right)\frac{\partial T}{\partial r} + \left(u\frac{\partial w}{\partial r} + w\frac{\partial w}{\partial z}\right)\frac{\partial T}{\partial z}\right) + q^* \tag{6}$$

Where $q^* = \frac{k_\infty U_w}{z\nu(\rho c)_f}\{A^*(T_w - T_\infty)f + B^*(T - T_\infty)\}$ (7)

$$u\frac{\partial C}{\partial r} + w\frac{\partial C}{\partial z} = D_B\left(\frac{\partial^2 C}{\partial r^2} + \frac{\partial^2 C}{\partial z^2} + \frac{1}{r}\frac{\partial C}{\partial r}\right) + \frac{D_T}{T_\infty}\left(\frac{\partial^2 T}{\partial r^2} + \frac{\partial^2 T}{\partial z^2} + \frac{1}{r}\frac{\partial T}{\partial r}\right) \tag{8}$$

Where the kinetic energy is equal to $\frac{\mu_f}{\rho_f}$. Here μ_f stands for the dynamic viscosity and the base liquid density ρ_f, $\alpha_m = \frac{k_1}{(\rho c)_f}$ stands for the thermal diffusivity, here thermal conductivity represented by k_1, the liquid heat capacity and nanoparticle heat capacity are represented by $(\rho c)_f$ and $(\rho c)_p$ respectively, Casson parameter β, the temperature of the fluid is represented by T, the concentration of nano-size metallic particles is by C, λ_2 is Thermal relaxation factor, q^* is the non

uniform heat source/sink, A^*, B^* are source and sink coefficients respectively.D_T, D_B are Brownian diffusion co-efficient, and Thermophoresis diffusion co-efficient respectively.

The boundary conditions are expressed as the energy levels of the fluid.

At z=0 : $u = L_1 \frac{\partial u}{\partial z}$ $\mathrm{v} = \mathrm{L}_1 \frac{\partial \mathrm{v}}{\partial \mathrm{z}} + r\Omega$, $\mathrm{w} = 0$, $\mathrm{T} = \mathrm{T_w} + \mathrm{L}_2 \frac{\partial \mathrm{T}}{\partial \mathrm{z}}$, $D_B \frac{\partial C}{\partial z} + \frac{D_T}{T_\infty} \frac{\partial T}{\partial z} = 0$

As z→ ∞: $u \to 0$, $T \to T_\infty, C \to C_\infty$, $P \to P_\infty$ (9)

Here, L_1, L_2represent the velocity slip, thermal slip respectively, and we introduce the similarity transformations

$$u(\eta) = r\Omega f'(\eta) \quad v(\eta) = r\Omega g(\eta) \quad w(\eta) = -2\sqrt{\Omega \nu}\, f(\eta) \quad \eta = \sqrt{\frac{\Omega}{\nu}}\, z$$

$$\theta(\eta) = \frac{T - T_\infty}{T_w - T_\infty} \varphi(\eta) = \frac{C - C_\infty}{C_w - C_\infty} P(\eta) = \frac{P_\infty - P}{\Omega \mu_f} \quad (10)$$

Where η is the similarity variable$f(\eta), g(\eta)$ are represented as non-dimensional velocities and, $\theta(\eta)$, $\phi(\eta)$ are the dimensional temperature function, and dimensionless concentration function respectively. Equation (2) is already satisfied by equation (10), now eqns (3), (4), (5), (6), (7) and (8) becomes

$$\left(1 + \frac{1}{\beta}\right) f''' - f'^2 + 2ff'' + g^2 - Mf' - Kf' - Frf'^2 = 0 \quad (11)$$

$$\left(1 + \frac{1}{\beta}\right) g'' - f'g + fg' - Mg - Kg - Frg^2 = 0 \quad (12)$$

$$\theta'' + 2P_r f\theta' + P_r(N_b \theta'\phi' + N_t \theta'^2 + \gamma_1(f^2\theta'' + ff'\theta') + Af + B\theta = 0 \quad (13)$$

$$\phi'' + 2P_r Lef\phi' + \frac{N_t}{N_b}\theta'' = 0 \quad (14)$$

Similarly, boundary conditions are transferred into

$$\eta = 0 \Rightarrow f = 0,\ f' = \gamma f'',\ g = 1 + \gamma g',\ \theta = 1 + \alpha\theta', \phi' + \frac{N_t}{N_b}\theta' = 0$$

$$\eta \to \infty \Rightarrow f' \to 0, g \to 0,\ \theta \to 0,\ \phi \to 0 \quad (15)$$

Here $M = \frac{\sigma_f B_0^2}{\rho_f \Omega}$ for the magnetic parameter, $K = \frac{\nu}{k^* \rho_f \Omega}$ for the porosity parameter, $Fr = \frac{F_r}{\rho_f}$ for the Forchheimer parameter, $P_r = \frac{\nu}{\alpha_m}$ prandlt number, $N_b = \left(\frac{(\rho c)_p}{(\rho c)_f}\right)\left(\frac{D_B}{\nu}\right)(C_w - C_\infty)$ for Brownian parameter $N_t = \left(\frac{D_T}{\nu}\right)(T_w - T_\infty)$ for Thermophoresis parameter, $\gamma_1 = 4\lambda_2\Omega$ for the Thermal relaxation time, $A = A^*\left(\frac{k_\infty U_w}{z\nu(\rho c)_f}\right)(T_w - T_\infty)$, $B = B^*\left(\frac{k_\infty U_w}{z\nu(\rho c)_f}\right)$ are represented as space, temperature-dependent heat generation and absorption parameters respectively, $L_e = \frac{\alpha_m}{D_B}$ for lewis number, $\gamma = L_1\sqrt{\frac{2\Omega}{\nu}}$ for velocity slip parameter, $\alpha = L_2\sqrt{\frac{2\Omega}{\nu}}$ for thermal slip parameter.

Mass transfer, heat transfer, and non-dimensional skin friction rates can be expressed.

$$Re_r^{\frac{1}{2}}C_f = f'(0), \quad Re_t^{\frac{1}{2}}C_g = g'(0), \; Re_r^{\frac{-1}{2}}Nu = -\theta'(0), \; Re_r^{\frac{-1}{2}}Sh = \phi'(0) \qquad (16)$$

Where the Reynolds number is calculated by taking into account the $Re_r = \frac{2(r\,\Omega)}{\nu}$.

3. Numerical Procedure

A convenient shooting method is used to treat the boundary conditions [15] of the fluid. For the initial value problems [11] to [14], we can substitute the numbers $y_1 = f\,, y_2 = f', y_3 = f'', y_4 = g, y_5 = g', y_6 = \theta, y_7 = \theta',\; y_8 = \phi, y_9 = \phi'$. we then obtained the following initial value problems into first-order differential equations.

$$y_1' = y_2; \quad y_2' = y_3; \; y_3' = \frac{1}{\left(1+\frac{1}{\beta}\right)}(y_2^2 - 2y_1y_3 - y_4^2 + My_2 \; + Ky_2 + Fry_2^2);$$

$$y_4' = y_5\,; \; y_5' = \frac{1}{\left(1+\frac{1}{\beta}\right)}(y_2y_4 - y_1y_5 + My_4 + Ky_4 + Fry_4^2); \; y_6' = y_7;$$

$$y_7' = -\frac{Pr}{1+Pr\gamma_1y_1^2}(2y_1y_7 + N_by_7y_9 + N_ty_7^2 + \gamma_1y_1y_2y_7 + Ay_1 + By_1);$$

$$y_8' = y_9; \; y_9' = -2PrLey_1y_9 - \frac{N_t}{N_b}\,\theta''$$

Boundary conditions can be transformed as follows

$$y_1(0) = 0, \;\; y_2(0) = \gamma s_1 \;\; , \;\; y_3(0) = s_1, \;\; y_4(0) = 1 + \gamma s_2, y_5(0) = s_2, y_6(0) = 1 + \alpha s_3, \;\; y_7(0) = s_3, y_8(0) = s_4, y_9(0) = -\left(\frac{N_t}{N_b}\right)y_7(0), y_2(\infty) \to 0, y_4(\infty) \to 0, \;\; y_6(\infty) \to 0, \;\; y_8(\infty) \to 0$$

The fifth-order RK-technique has been utilized to integrate the given equations.$s_1, s_2, s_3 \; and \; s_4$ are the initial values of the slope while integrating the above system. The slopes $s_1, s_2, s_3 \; and \; s_4$ are iteratively by using Newton method. Numerical results are evaluated at $\eta_{max} = 20$ For the scope of slip parameters, this method fulfills the far-field conditions. We were able to obtain numerical results from bvp4c of MATLAB.

4. Numerical outcomes and conversation

This paper visualizes the scope of slip parameters' features can be represented in equations (11) - (14) namely, porosity parameter, Forchhiemer flow parameter, magnetic parameter, Casson fluid parameter, Prandtl number, Brownian motion parameter, Thermophoresis parameter, Lewis number against radial velocity profile, tangential velocity, temperature distribution profile and volumetric concentration profile. Controlling of flow parameters has a few study ranges such as $0 < M < 1$, $0 < Fr < 1, 0 < K < 1$ etc. Here combined porosity and magnetic parameters. The study of the various aspects of the magnetic properties of a medium that's used in the flow of nanofluids is carried out. Fig.1 The exact nature of M can also be determined by comparing its properties with that of the radial velocity field$f'(\eta)$. The velocity distribution of a revolving disk can be affected by the upper limit of the magnetic parameter influence. As its resistivity and Lorentz force increase, the effects of this variable's rise become more apparent. Fig. 2 illustrates the effect of the magnetic parameter M on the distribution of the tangential velocity$g(\eta)$. It shows that increasing its value causes the velocity distribution to decrease. The performance of the Casson parameter β is evaluated

in terms of its relation to the radial velocity $f'(\eta)$ in Fig.3. Magnitude variations in the parameter's value can cause a drop in the velocity profile of $f'(\eta)$.

The plot presented in Fig. 4 shows the Casson parameter β value relative to the distribution of the tangential velocity $g(\eta)$. The value decrease shown in $g(\eta)$ is an interesting aspect of the plot. The Darcy-Forchheimer parameter Fr influence on the Radial velocity $f'(\eta)$ speed profile is shown in Fig. 5. The reduction in the profile is the result of higher estimates for this parameter. The Fig.6 shows Fr variable's identifiable speed circulation range in the tangential velocity $g(\eta)$. The distribution and other layers speed profile also decreased due to the expanding value. Fig.7 shows the various K permeability factor estimates made using a rotating disc's distribution of Nanofluid. Since K increases $f'(\eta)$ decreases for the nano fluid we understood here that the higher values of permeability constraint indicate lower permeability of the porous medium. The consequence of raising the porosity parameter K is shown in Fig. 8, whereby the nanofluid's flow g(η) decreases.

Fig.9 The thermal relaxation coefficient γ_1 influences the temperature profile $\theta(\eta)$ of a fluid. High values of this parameter can cause the fluid's temperature to decrease. Its insulating properties can help in reducing the temperature. The distribution of temperatures is also studied by analyzing how A and B, as well as the sink and heat source, affect this phenomenon.

In Fig.10 &11The increasing values of A and B can cause the temperature profile$\theta(\eta)$ to rise. The heat source parameter can then cause the nanofluid to generate more heat. The Brownian factor known as Nb influences the temperature profile $\theta(\eta)$ by determining its distribution. Another well-known thermal and spatial parameter, the Prandtl number Pr, shows the transfer rate of heat from a solid to a flowing liquid. Temperature profiles begin to decrease as the Prandtl numbers are raised in Fig.12.

The distribution of concentration profile $\phi(\eta)$ across Fig.13 shows a decreasing trend as the Prandtl number Pr increases. The relationship between conductivity and thermal diffusivity can be represented by the Prandtl number. Because of this, the increased Prandtl values can cause thermal diffusivity to decrease. Fig.14 depicts the random motion of microscopic particles increases as the Brownian moment factor rises. The heightened random Brownian motion Nb leads to increased collisions among nano particles, causing the conversion of kinetic energy into heat energy. Consequently; an increase the Brownian motion factor Nb results in an elevated temperature distribution with in fluid. Fig.15 The concentration profile $\phi(\eta)$ can be described as a distinct characteristic by increasing Nb values.

The relationship between the concentration profile $\phi(\eta)$ and temperature distribution $\theta(\eta)$ can be shown in Fig.16. It's revealed that the thermophoresis factor Nt causes an increase in this parameter's profile. A plot against Fig.17 shows the Nt features and how they affect the distribution. In Fig.18 the concentration distribution $\phi(\eta)$ and the Lewis parameter Le can be moved together to show the relationship between their values. It's important to note that the rising Le value causes a decrease in the distribution. This illustrates the link between the various features of Pr and the concentration field.

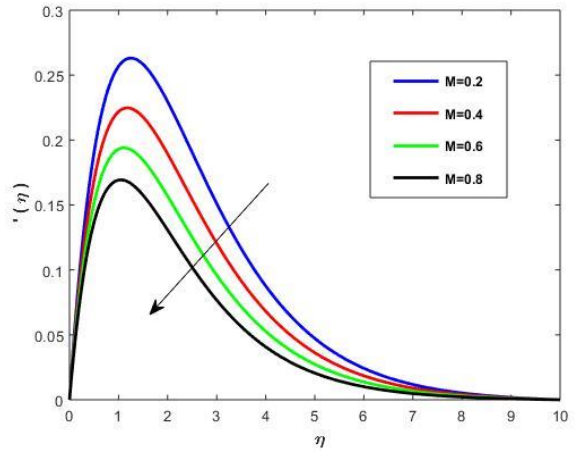

Fig.1 Impact of M on radial velocity$f'(\eta)$.

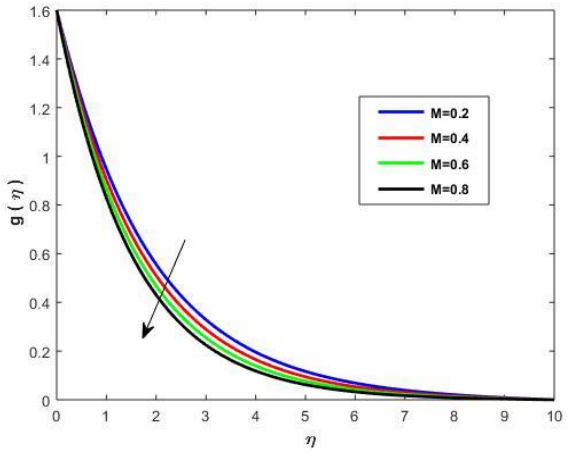

Fig. 2 Impact of M on tangential velocity $g(\eta)$.

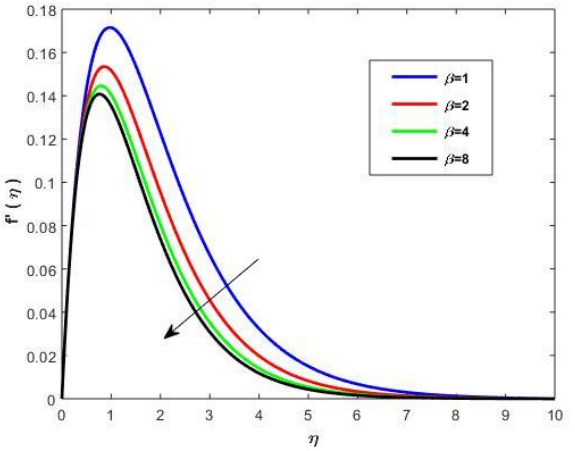

Fig.3 Impact of Casson parameter β on $f'(\eta)$.

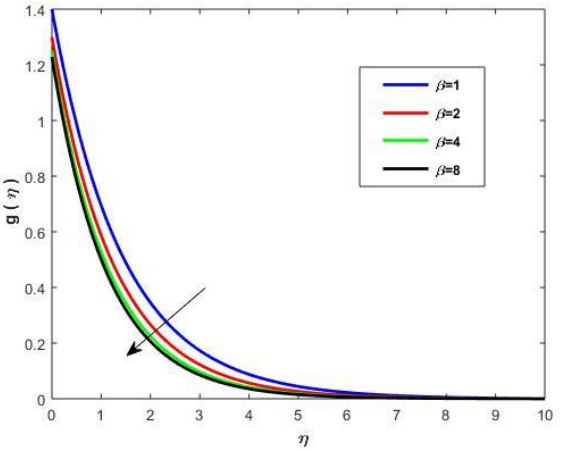

Fig.4 Impact of Casson parameter β on $g(\eta)$

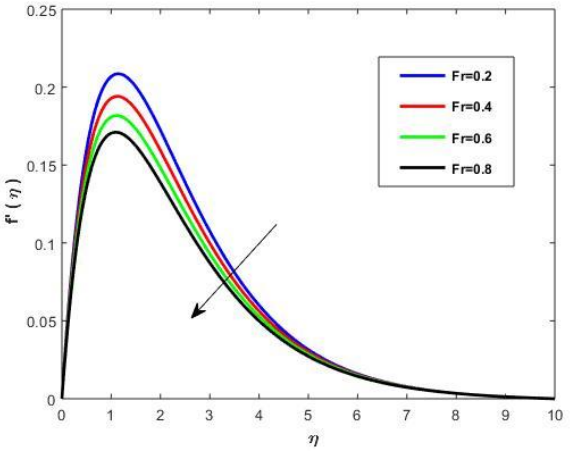

Fig.5 Various of Forchhiemer parameter Fr on $f'(\eta)$.

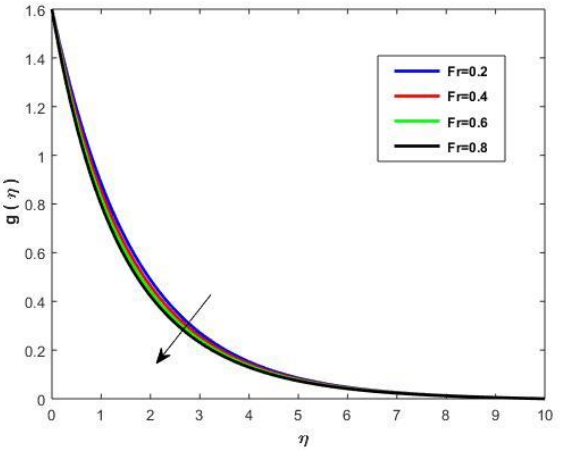

Fig.6 Various of Forchhiemer parameter Fr on $g(\eta)$

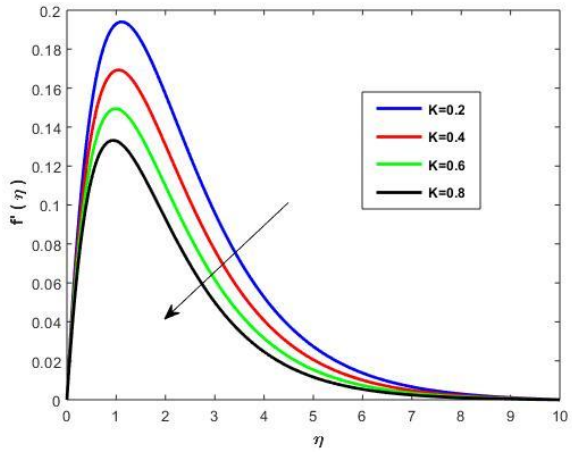

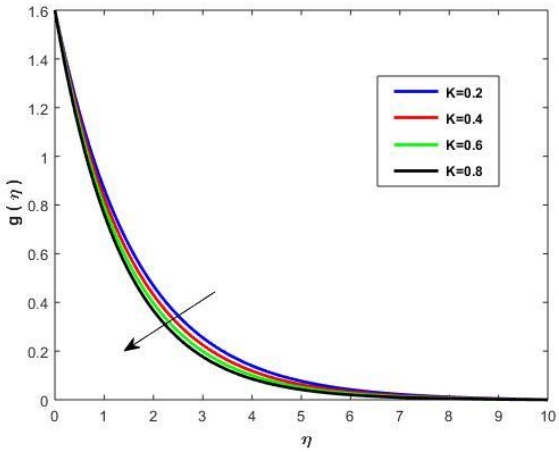

Fig.7 Impact of Porosity parameter K on radial velocity $f'(\eta)$. Fig.8 Impact of Porosity parameter K on $g(\eta)$

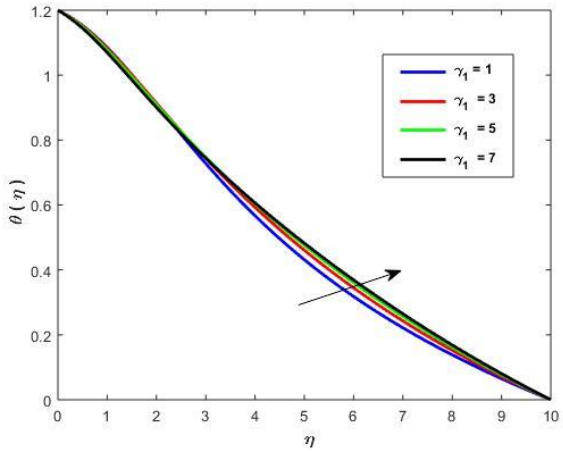

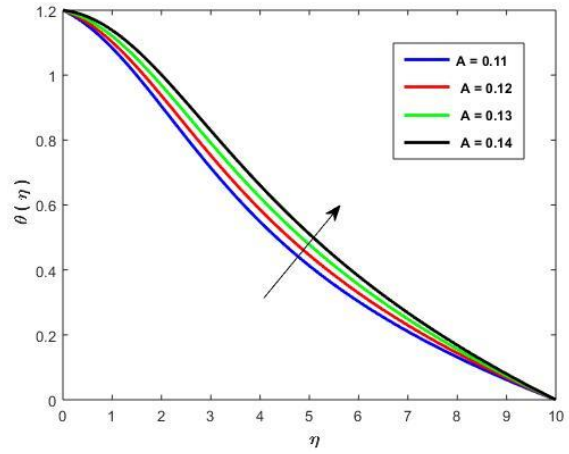

Fig.9 Influence of Thermal relaxation parameter γ_1 on $\theta(\eta)$. Fig.10 Influence of heat source parameter A on $\theta(\eta)$

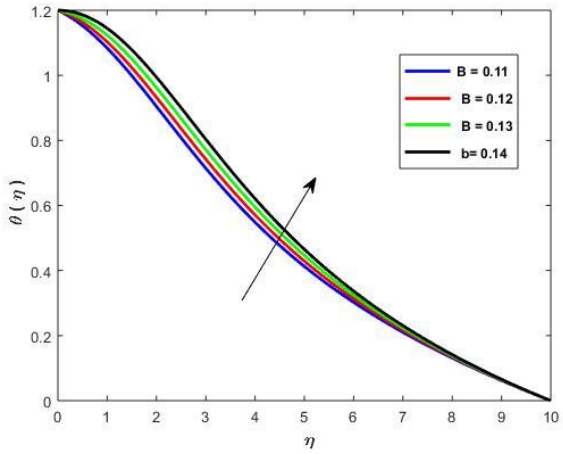

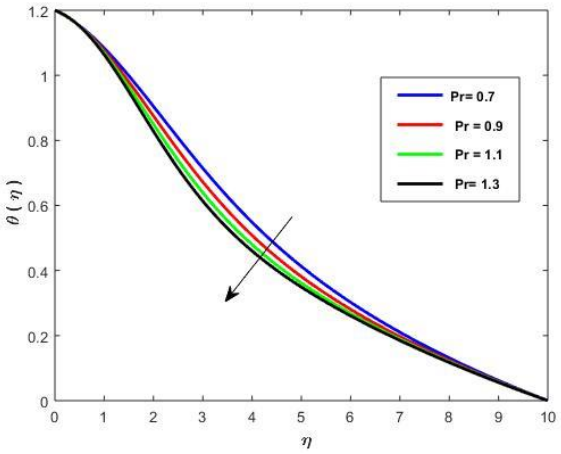

Fig.11 Influence of heat sink parameter B on $\theta(\eta)$. Fig.12 Influence of Prandtl number Pr on $\theta(\eta)$

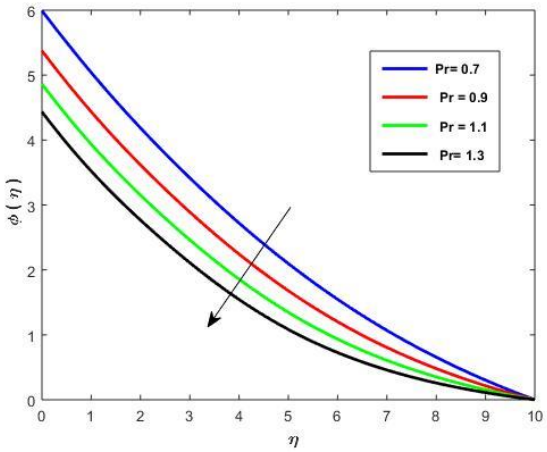

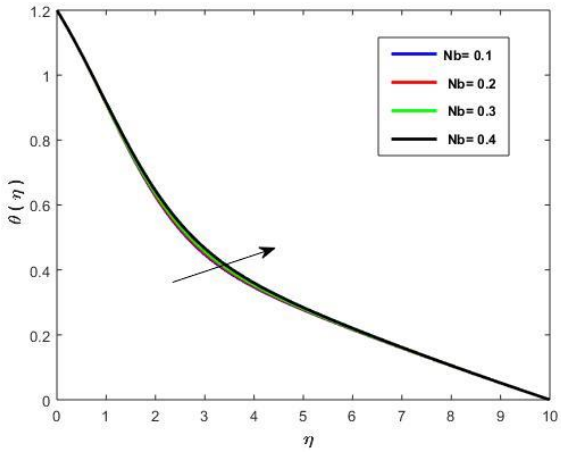

Fig.13 Influence of Prandtl number Pr on $\phi(\eta)$. Fig.14 Influence of Brownian factor Nb on $\theta(\eta)$

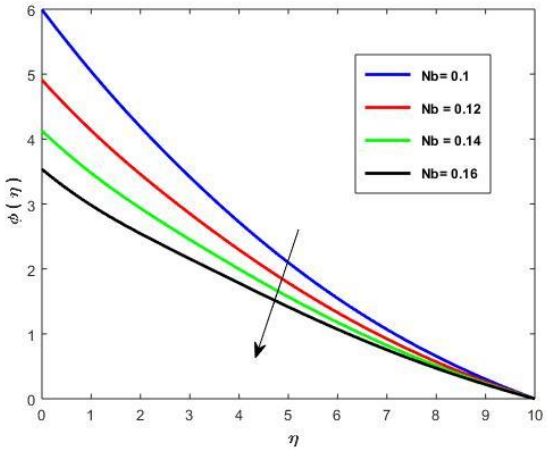

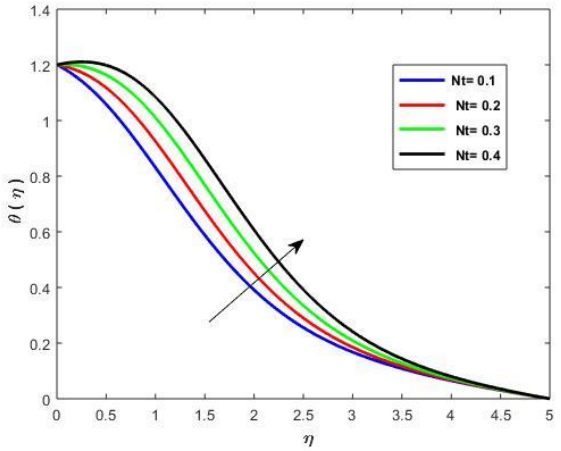

Fig. 15 Influence of Brownian factor Nb on $\phi(\eta)$. Fig.16 Influence of Thermophoresis parameter Nt on $\theta(\eta)$

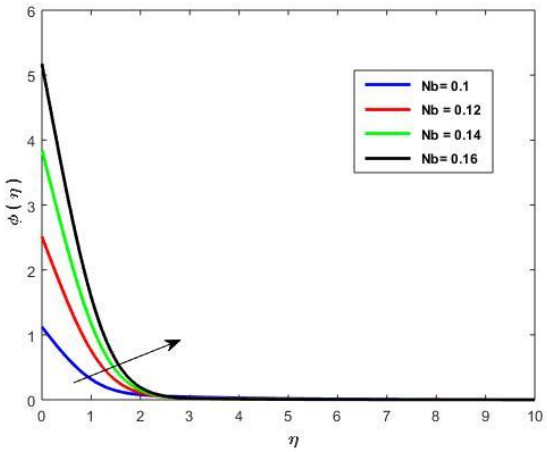

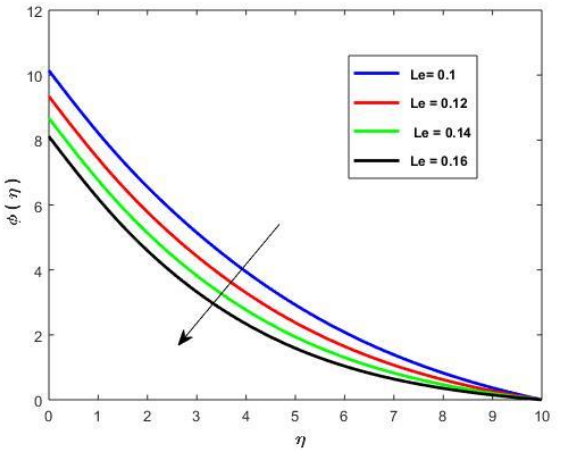

Fig.17 Influence of Thermophoresis parameter Nt on $\phi(\eta)$. Fig.18 Influence Lewis number Le on $\phi(\eta)$.

Table 1. Computational values of radial velocity $f'(\eta)$, tangential velocity $g(\eta)$ computed against various estimates M, K, Fr, α, β, γ

M	K	Fr	β	α	γ	$f'(\eta)$	$g(\eta)$
0.2	0.2	0.2	-	0.2	0.2	0.49356	0.88414
0.4						0.44601	0.98320
0.6						0.40793	1.07683
0.8						0.37703	1.16536
	0.4					0.44601	0.98320
	0.6					0.40793	1.07683
	0.8					0.37703	1.16536
		0.4				0.47187	0.96897
		0.6				0.45304	1.04822
		0.8				0.40295	0.72191
			2			0.50974	0.91313
			4			0.53311	0.95498
			7			0.49356	0.88414
				0.3		0.48231	0.92732
				0.5		0.46214	1.00923
				0.7		0.44452	1.08605
					0.2	0.44601	0.98320
					0.4	0.40793	1.07683
					0.6	0.37703	1.16536

Table 2. Numerical values of $-\theta'(0)$ computed against various estimates Pr, Nb, Nt, Le, A, B, γ_1, α, β

Pr	Nb	Nt	A	B	γ_1	α	β	Le	$-\theta'(0)$
0.3	0.3	0.1	0.1	0.1	0.1	0.2	0.2	0.1	0.08928
0.5									0.08587
0.9									0.07984
	0.1								0.06065
	0.2								0.07032
	0.4								0.09500
		0.2							0.01321
		0.3							0.02861
		0.4							0.06584
			0.15						0.02451
			0.2						0.03524
			0.25						0.09572

				0.15					0.01347
				0.2					0.14270
				0.25					0.33113
					3				0.08814
					5				0.09439
					7				0.10154
						1			0.08410
						4			0.09109
						7			0.10154
							0.2		0.02705
							0.3		0.14069
							0.4	0.1	0.25694

5. Conclusions

The researchers studied the swirling disk with a Casson nanofluid in the presence of a Cattaneo-Christov thermal flux. They found that the disk's flow and the associated boundary conditions have convective effects. The findings of the study support the use of bvp4c for solving the boundary value problem numerically.

(i) The temperature profile decreases with higher estimates of the thermal relaxation parameter.
(ii) Raising the fluid's temperature allows the researchers to calculate the sink or heat source parameter that is non-uniform.
(iii) The increase in the Brownian motion and Prandtl number parameter's values leads to a reduction of the heat field. On the other hand, the value of Nt increases.
(iv) The study demonstrates that the nanoparticle concentration decreases with the help of the enhanced slip parameter and Brownian motion.

References

[1] Copley, A. (1974). Hemorheological aspects of the endothelium-plasma interface. Microvascular Research, 8(2), 192–212. https://doi.org/10.1016/0026-2862(74)90094-6
[2] Blair, G. W. S. (1959). An Equation for the Flow of Blood, Plasma and Serum through Glass Capillaries. Nature, 183(4661), 613–614. https://doi.org/10.1038/183613a0
[3] Nadeem, S., Haq, R. U., & Lee, C. (2012). MHD flow of a Casson fluid over an exponentially shrinking sheet. Scientia Iranica, 19(6), 1550–1553. https://doi.org/10.1016/j.scient.2012.10.021
[4] Kandasamy, A., & Pai, R. G. (2011). Entrance Region Flow of Casson Fluid in a Circular Tube. Applied Mechanics and Materials, 110–116, 698–706. https://doi.org/10.4028/www.scientific.net/amm.110-116.698
[5] Jabbar, N., Hafeez, M. B., Askar, S., & Nazir, U. (2021). Non-Coaxially Rotating Motion in Casson Martial along with Temperature and Concentration Gradients via First-Order Chemical Reaction. Energies, 14(22), 7784. https://doi.org/10.3390/en14227784
[6] Alqarni, M. M., Bilal, M., Allogmany, R., Tag-Eldin, E., Ghoneim, M. E., & Yassen, M. F. (2022). Mathematical analysis of casson fluid flow with energy and mass transfer under the influence of activation energy from a non-coaxially spinning disc. Frontiers in Energy Research, 10. https://doi.org/10.3389/fenrg.2022.986284
[7] Von Karman T. Uber laminar and turbulent Reibung. *Z Angew Math Mech* 1921; 1: 233–255.

[8] Cochran, W. G. (1934). The flow due to a rotating disc. Mathematical Proceedings of the Cambridge Philosophical Society, 30(3), 365–375. https://doi.org/10.1017/s0305004100012561
[9] Benton ER. On the flow due to a rotating disk. *J Fluid Mech* 1966; 24: 781–800.
[10] Freidoonimehra, N., Rashidib, M. M., Khand, M. S., & Ferdowse, M. (2015). Soret and Dufour effects in an MHD flow over a porous rotating disk using HAM.
[11] Mustafa, M. (2017). MHD nanofluid flow over a rotating disk with partial slip effects: Buongiorno model. International Journal of Heat and Mass Transfer, 108, 1910–1916. https://doi.org/10.1016/j.ijheatmasstransfer.2017.01.064
[12] Shehzad, S., Abbas, Z., Rauf, A., & Abdelmalek, Z. (2021). Dynamics of fluid flow through Soret-Dufour impacts subject to upward and downward motion of rotating disk. International Communications in Heat and Mass Transfer, 120, 105025. https://doi.org/10.1016/j.icheatmasstransfer.2020.105025
[13] Kumar, M., & Mondal, P. K. (2022). Irreversibility analysis of hybrid nanofluid flow over a rotating disk: Effect of thermal radiation and magnetic field. Colloids and Surfaces a Physicochemical and Engineering Aspects, 635, 128077. https://doi.org/10.1016/j.colsurfa.2021.128077
[14] Ali, I., Gul, T., & Khan, A. (2023). Unsteady Hydromagnetic Flow over an Inclined Rotating Disk through Neural Networking Approach. Mathematics, 11(8), 1893. https://doi.org/10.3390/math11081893
[15] Shenoy, A. V. (1993). Darcy-Forchheimer natural, forced and mixed convection heat transfer in non-Newtonian power-law fluid-saturated porous media. Transport in Porous Media, 11(3), 219–241. https://doi.org/10.1007/bf00614813
[16] Sadiq, M. A., & Hayat, T. (2016). Darcy–Forchheimer flow of magneto Maxwell liquid bounded by convectively heated sheet. Results in Physics, 6, 884–890. https://doi.org/10.1016/j.rinp.2016.10.019
[17] Ganesh, N. V., Hakeem, A. A., & Ganga, B. (2018). Darcy–Forchheimer flow of hydromagnetic nanofluid over a stretching/shrinking sheet in a thermally stratified porous medium with second order slip, viscous and Ohmic dissipations effects. Ain Shams Engineering Journal, 9(4), 939–951. https://doi.org/10.1016/j.asej.2016.04.019
[18] Sadiq, M., Waqas, M., & Hayat, T. (2017). Importance of Darcy-Forchheimer relation in chemically reactive radiating flow towards convectively heated surface. Journal of Molecular Liquids, 248, 1071–1077. https://doi.org/10.1016/j.molliq.2017.10.063
[19] Khan, M. I., Alzahrani, F., Hobiny, A., & Ali, Z. (2020). Estimation of entropy optimization in Darcy-Forchheimer flow of Carreau-Yasuda fluid (non-Newtonian) with first order velocity slip. Alexandria Engineering Journal, 59(5), 3953–3962. https://doi.org/10.1016/j.aej.2020.06.057
[20] Rasool, G., Shafiq, A., Wang, X., Chamkha, A. J., & Wakif, A. (2023). Numerical treatment of MHD Al2O3–Cu/engine oil-based nanofluid flow in a Darcy–Forchheimer medium: Application of radiative heat and mass transfer laws. International Journal of Modern Physics B. https://doi.org/10.1142/s0217979224501297
[21] Nayak, M., Shaw, S., Khan, M. I., Pandey, V., & Nazeer, M. (2020). Flow and thermal analysis on Darcy-Forchheimer flow of copper-water nanofluid due to a rotating disk: A static and dynamic approach. Journal of Materials Research and Technology, 9(4), 7387–7408. https://doi.org/10.1016/j.jmrt.2020.04.074
[22] Waqas, H., Naseem, R., Muhammad, T., & Farooq, U. (2021). Bioconvection flow of Casson nanofluid by rotating disk with motile microorganisms. Journal of Materials Research and Technology, 13, 2392–2407. https://doi.org/10.1016/j.jmrt.2021.05.092
[23] Lv, Y. P., Gul, H., Ramzan, M., Chung, J. D., & Bilal, M. (2021). Bioconvective Reiner–Rivlin nanofluid flow over a rotating disk with Cattaneo–Christov flow heat flux and entropy generation analysis. Scientific Reports, 11(1). https://doi.org/10.1038/s41598-021-95448-y